

P5.17 GLOBAL OPERATIONAL SEA SURFACE TEMPERATURE AND AEROSOL PRODUCTS FROM AVHRR: CURRENT STATUS, DIAGNOSTICS, AND POTENTIAL ENHANCEMENTS

Alexander Ignatov^{*1}, John Sapper², Istvan Laszlo¹, Nicholas Nalli^{1,3}, Andrew Harris^{1,4}
William Pichel¹, Alan E. Strong¹, Eric Bayler¹, Xiaofeng Li^{1,5}, Eileen Maturi¹

¹NOAA/NESDIS/ORA, Camp Springs, MD

²NOAA/NESDIS/OSDPD, Suitland, MD

³QSS Group Inc, Camp Springs, MD

⁴University of Maryland, College Park, MD

⁵DSTI Inc, Camp Springs, MD

1. BACKGROUND

Three generations of the Advanced Very High Resolution Radiometers, AVHRR/1 to 3, have been flown onboard TIROS-N/NOAA Polar Operational Environmental Satellites (POES) since 1978. Specifics of the POES sun-synchronous orbits, and AVHRR instruments are discussed in sections 2 and 3 below.

Based on an extensive theoretical radiative transfer analysis of sea surface temperature (SST, or T_s) retrievals, including that of McMillin (1975), NESDIS had developed and successfully implemented its all-time-first global operational multi-channel SST (MCSST) product upon the successful launch of the first AVHRR/2 instrument onboard NOAA-7 in 1981 (McClain et al. 1985). In 1990, with launch of NOAA-11, a non-linear SST (NLSST) product replaced the MCSST (Walton et al. 1998).

The MC/NLSST equations are applied only to those AVHRR pixels which have been navigated, calibrated, cloud screened and quality controlled. Currently, these pre-processing functions are performed at NESDIS within a complex mainframe-based system called the Main Unit Task (MUT). The success of the NESDIS SST operational production is largely due the MUT system which has proven robust and flexible. It was later adopted at the Naval Oceanographic Office (NAVOCEANO) as a part of the Shared Processing Program (May et al. 1997). The MUT system is briefly summarized in section 4.

Simultaneously with NLSST, NESDIS followed earlier studies by Griggs (1975) and launched another highly successful operational product from the AVHRR over the global ocean, the aerosol optical depth (AOD, or τ) (Rao et al. 1989). AVHRR data in the solar reflectance bands (SRB), processed within the same MUT system, are utilized for the τ -retrievals. Since its inception, three versions (or "generations") of the NESDIS aerosol product have been implemented. As of today, it remains the only operational real-time aerosol product in the world. More recently, AVHRR-like aerosol algorithms have been enhanced and applied to data

from other sensors (TRMM VIRS, *Terra/Aqua* MODIS, and MSG/SEVIRI) under the CERES project (Ignatov et al 2004ab).

Currently, operational SST and aerosol retrievals are made from the two platforms, NOAA-16 and -17. The SST and AOD products are discussed in sections 4-5, and illustrated by a case study from 3-11 December 2003.

Note that although the SST and AOD retrievals are made within the same MUT system, their respective sampling domains differ significantly. Aerosol retrievals are not made during nighttime and in areas contaminated by sun-glint (defined as an area within a 40° glint angle cone around the specular point), and on the solar side of the orbit. For this study, we have chosen to analyze a combined SST/aerosol sample, in which each observation contains both τ and T_s retrievals.

Although the SST equations and aerosol look-up-tables have progressed through a number of improvements (generations) over years, the MUT system designed in the early 1980s has remained largely unchanged. Recently, NESDIS took the initiative to fund a fundamental redesign of the MUT system. The AVHRR/3 is scheduled to fly on at least one more US platform, NOAA-N (to be launched in Feb 2005 into an afternoon orbit to replace NOAA-16, whose AVHRR has experienced technical problems during most of 2004 (<http://www.oso.noaa.gov/poesstatus/>)). Three European platforms METOP1-3 carrying the AVHRR/3 sensor will be launched into morning orbits in December 2005, 2010, and 2014, respectively. With a nominal platform life time of ~5 years, this would add another 15+ years to the current 20+ year AVHRR record, to potentially comprise a comprehensive SST/aerosol climate data record (CDR).

2. NOAA ORBITAL CONFIGURATION

NOAA strives to keep at least two platforms in sun-synchronous orbits at all times, by launching new satellites to replace the aged ones. These orbits have been carefully chosen to allow four measurements per day approximately equidistant in time, at the same local solar time (LT), to provide for consistent scene illumination and segment of the diurnal cycle. One platform is termed *morning* and the other *afternoon*, with orbital planes about 90° (six hours) apart along the

*Corresponding author address: Alexander Ignatov, E/RA3, Rm. 603, WWB, NOAA, 5200 Auth Rd., Camp Springs, MD 20746-4304; e-mail: Alex.Ignatov@noaa.gov

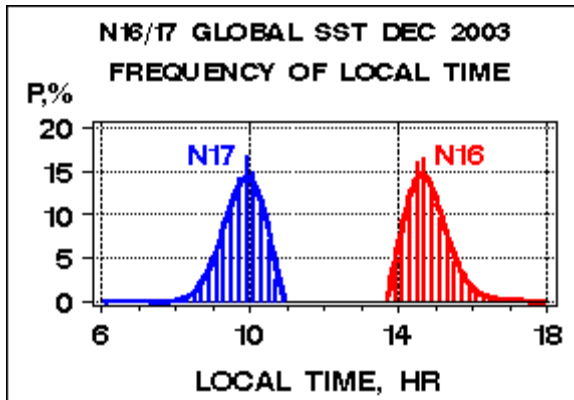


Fig.1. Frequency distribution of local time (LT) in the NOAA-16 and -17 SST/Aerosol files in December 2004.

approximate north-south axis. The *afternoon* satellites are launched in an “ascending” (northbound) orbit, with an Equator Crossing time (EXT, or η) of ~1500 (TIROS-N), ~1430 (NOAA-7,-9), ~1330 (NOAA-11,-14), or ~1400 (NOAA-16). These orbits “descend” from north to south on the dark side of Earth at (η -12)~0300, 0230, 0130 or 0200, respectively. The *morning* satellites “descend” from north to south at η ~0730, and “ascend” from south to north in the local evening, at (η +12)~1930. NOAA-17 is the first *mid-morning* satellite, with descending (southbound) node passing at η ~1000, and ascending (northbound) node occurring at (η +12)~2200. Data used in this study are from the AM pass of NOAA-17 and PM pass of NOAA-16, only, for which the illumination conditions are favorable for aerosol retrievals.

Note that the definitions of the *morning* and *afternoon* platforms, widely used in the community, should be considered a mere convention, to differentiate between the two types of orbits. This jargon may well appear confusing to a fresh user of the NOAA data. In particular, either platform has both an AM and PM pass (unlike what its name may suggest). Furthermore, the AM pass of a *morning* platform occurs while on a descending part of the orbit, whereas the PM pass of an

afternoon platform is on an ascending part. In fact, both platforms ascend from south to north in the local afternoon (η ~1330 and 1930), and descend back from north to south during the local morning (η ~0130 and 0730).

When using the EXT as a proxy for the LT of satellite sensor observation, two factors should be considered. First, the LT changes systematically with latitude, due to Earth rotation and orbit inclination, even for nadir views. Also, the cross-scanning AVHRR may “look” more than a thousand kilometers off nadir. An example of actual frequency distributions of the LT in the SST/Aerosol files analyzed in this study is shown in Fig.1. The observations are clustered around LT~1000 for NOAA-17 and LT~1430 for NOAA-16. [Recall that aerosol retrievals are taken on the anti-solar side of the orbit, only.]

Note also that the above EXTs are but target overpass times at launch, whereas the actual EXT systematically changes during satellite lifetime as shown in Figs.2-3 after (Ignatov et al. 2004a). In particular, NOAA-16 will be flying at η ~1500 by 2006, at η ~1600 by 2008, and at η ~1800 by 2011. According to Fig.3, the NOAA-17 EXT will reach its maximum of η_{max} ~1020 by 2005, then return back to the launch value of η ~1000 by 2007, and subsequently decline to η ~0900 by 2009 and further to η ~0800 by 2011. [Note that whatever the evolution of the EXT during lifetime of a platform, its *morning* or *afternoon* attributes designated at launch, remain unchanged.]

Data of Figs.1-3 suggest that the AVHRR SST and aerosol products are highly non-uniform in LT, and this non-uniformity evolves with time.

3. AVHRR INSTRUMENT

AVHRR/1 flown onboard TIROS-N, NOAA-6,-8,-10 had two solar reflectance bands (SRB) centered at 0.63 and 0.83 μ m (bands 1-2) and two Earth emission bands (EEB) centered at 3.7 and 11 μ m (3-4) (Kidwell 1998). [On the sunlit part of the orbit, band 3 is also sensitive to reflected solar radiation. Still, it is considered an EEB here from the standpoint of its calibration.]

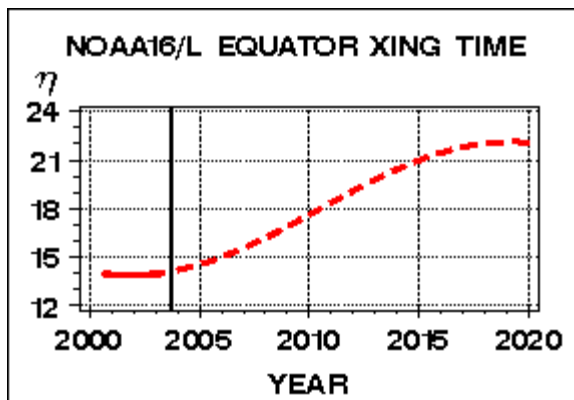


Fig.2. Local EXT for NOAA-16 (ascending/northbound node). Solid vertical line separates the past EXT prior to 2003, and its future projection beyond 2004.

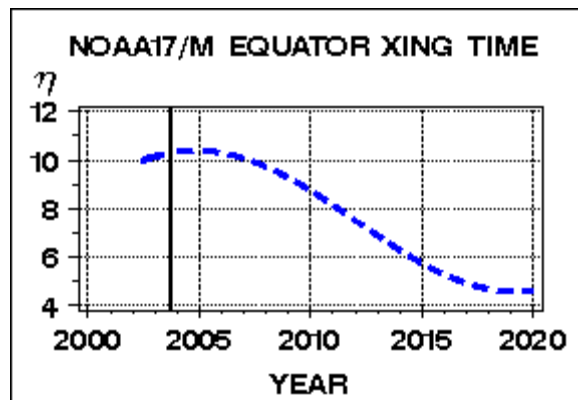


Fig.3. Local EXT for NOAA-17 (descending/southbound node; add 12h for ascending/northbound).

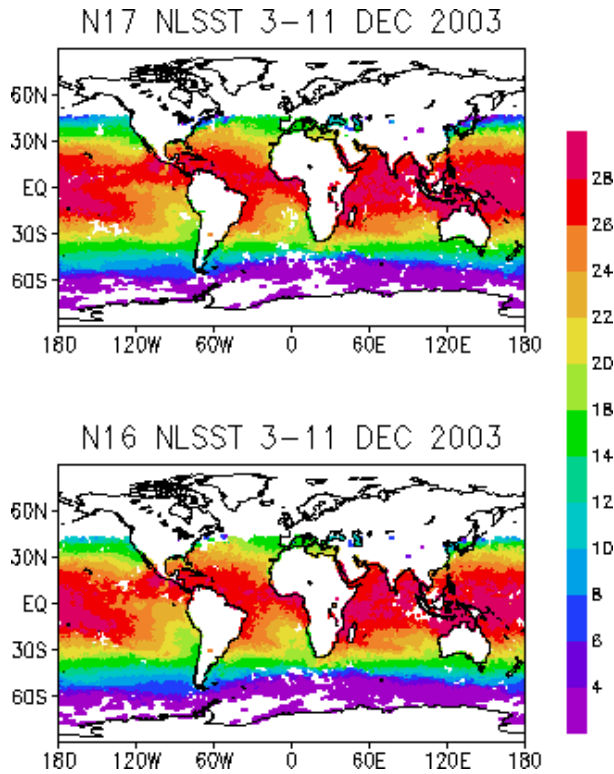


Fig.4. Global maps of SST derived from the morning (top: NOAA-17, EXT~1000) and afternoon (bottom: NOAA-16, EXT~1400) platforms.

AVHRR/2 (flown onboard NOAA-7,-9,-11,-12,-14) has an additional band 5 centered at $12 \mu\text{m}$. This split-window enhancement was critically important for SST retrievals during daytime, because of the above-mentioned solar contribution in band 3.

AVHRR/3 (flown onboard the current generation of NOAA-KLM satellites, NOAA-15 to 17, and to be flown on NOAA-N and three METOP platforms) is an improved instrument with the overall sensor design upgraded from AVHRR/2 (Goodrum et al. 2003). A larger external sun shield has been added to the scan motor housing to reduce sunlight impingement and associated calibration problems. An additional SRB was added centered at $1.61 \mu\text{m}$. The new band is termed 3A, because it shares a telemetry slot with the former band 3 @ $3.7 \mu\text{m}$ that is now termed 3B. The only platform where the 3A is currently used during daytime is NOAA-17. On NOAA-15 and -16, 3B is on (and hence 3A off) permanently. The primary reason for this is the use of 3B for fire detection, a task that is best performed in the afternoon due to burning habits. Another feature of the AVHRR/3 which is important for aerosol retrievals is a refined sensitivity in the SRBs at low radiances, achieved through the concept of a "dual-gain."

Note that the AVHRR instrument was primarily designed as a surface/cloud imager for weather applications. Its precision quantitative usage such as for SST and aerosol retrievals was not originally foreseen. The EEBs are calibrated onboard, via looking at the two calibration targets: an onboard high radiance black

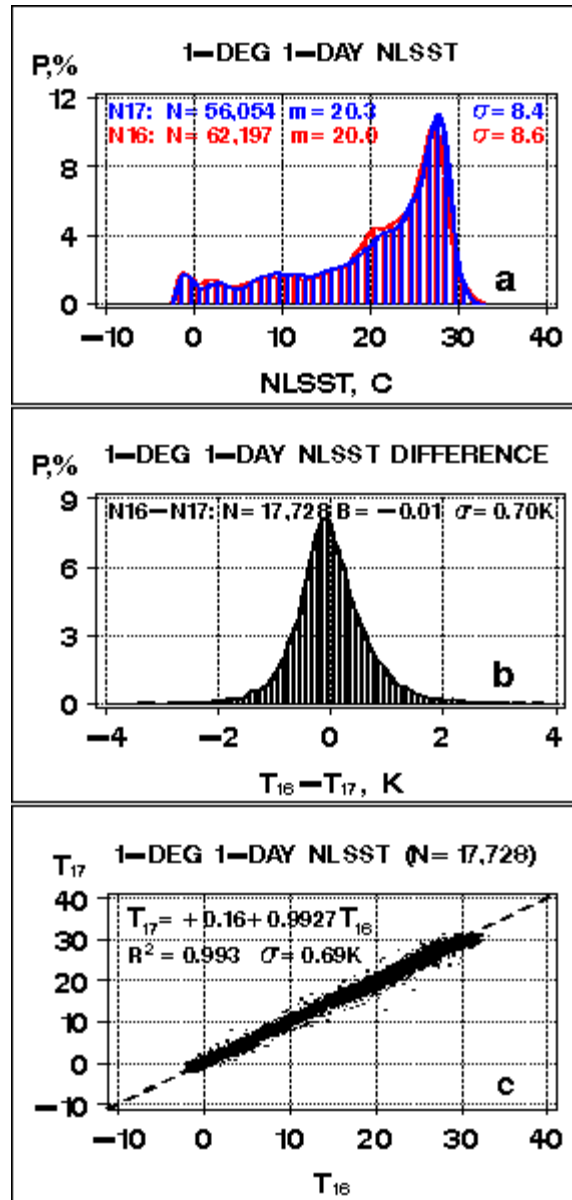


Fig.5. Global SST statistics: histograms of (a) T_{16} and T_{17} and (b) $T_{16}-T_{17}$; and (c) scattergrams T_{17} vs T_{16} .

body, and low (zero) radiance deep space. In the SRBs, however, only deep space is measured (note that this measurement is not presently used in the operational calibration), and there was no provision for a visible onboard calibration. Consequently, a stable vicarious target on the Earth's surface is customarily used to specify the high radiance calibration point and subsequently estimate the calibration slope (gain) in the SRBs (e.g. Rao and Chen 1995).

4. NESDIS MUT SYSTEM

The MUT system was set up at NESDIS in the early 1980s (McClain 1989), and it has basically remained

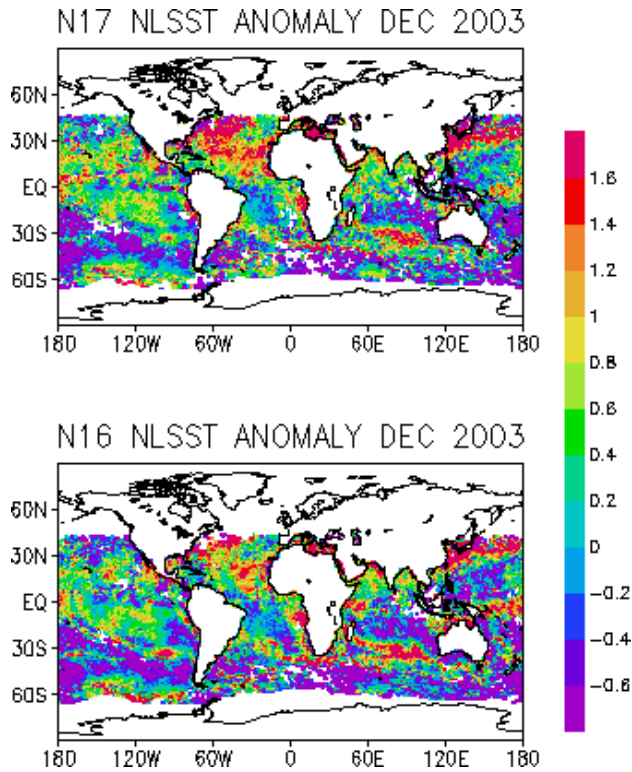


Fig.6. Same as in Fig.4 but for the SST anomalies.

unchanged in its overall structure and functionality. The MUT system consists of two subsystems: the SST (SSTOBS) and Aerosol (AEROBS) observations. Since the AEROBS system was added to the SSTOBS system, which had been already in existence for almost 10 years, the two subsystems share much in common.

The SST/AEROBS products reside on the NESDIS Central Environmental Monitoring Satellite Computer System (CEMSCS) as rotating files, one per product and platform. At each given point in time, each file contains all aerosol/SST retrievals during the last 8 days (approximately representing the full repeat cycle of a NOAA satellite). The files are renewed automatically 4 times a day, around 0100, 0700, 1300, and 1800 EST.

The MUT software receives Level 1b data as input, and processes them by "target." A target is defined as an 11x11 array of AVHRR 4 km global area coverage (GAC) fields-of-view (FOV) centered on the FOVs of the High-resolution Infra-Red Sounder (HIRS), an instrument flown synergistically alongside AVHRR onboard NOAA satellites (Kidwell 1998; Goodrum 2003). Approximately 60,000 targets per orbit, 14 orbits per day, are processed from each platform.

First, the quality control (QC) flags of the target (available from the Level 1b database) are checked. If certain fatal QC flags are tripped, processing of the target is terminated. A count of the number of QC errors is accumulated by blocks of 500 scan lines to allow bad sections of data to be identified for diagnostic study. The

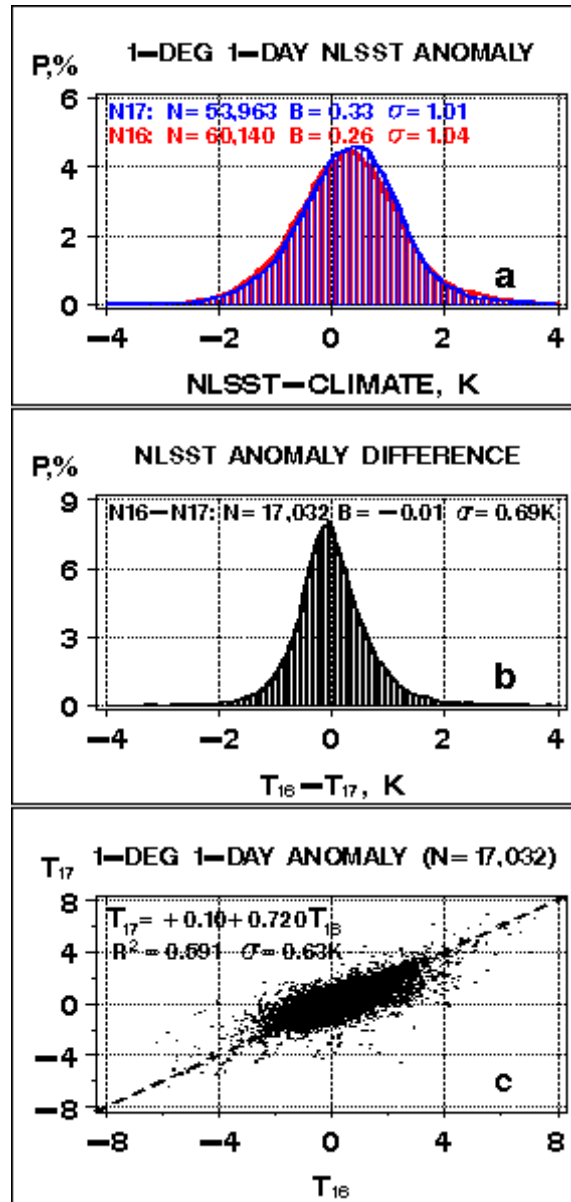


Fig.7. Same as in Fig.5 but for the SST anomalies.

magnitude and consistency of AVHRR and HIRS calibration coefficients are also monitored, and targets with erroneous calibration data are likewise rejected.

Next, one or more processing algorithms are selected: SST (daytime or nighttime), AOD, etc. [Note that a simultaneous parallel-test mode allows comparison of results from a new algorithm with the result of the operational algorithm, for a selected portion of the global ocean.] The processing algorithm includes identifying targets suitable for the retrievals, and performing the retrieval. The specific tests have been summarized by McClain et al. (1985), and their most up-to-date version is found in Ignatov et al. (2004b).

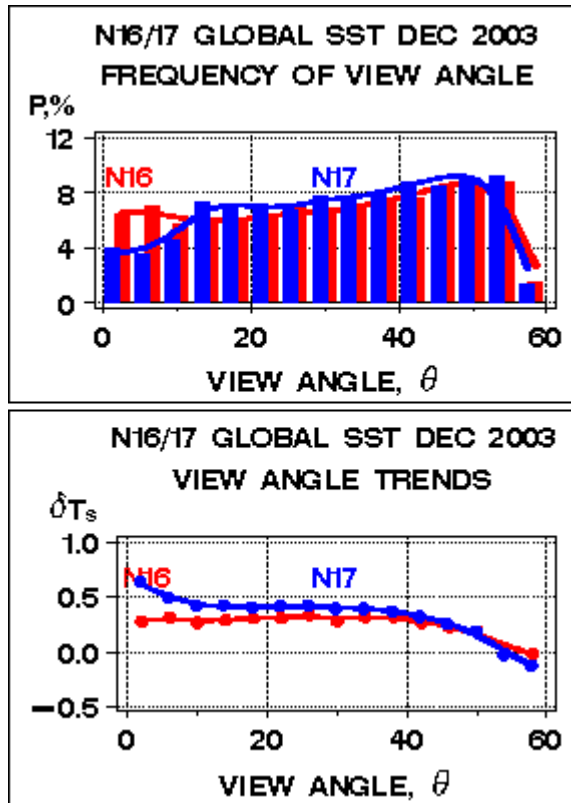


Fig.8. View zenith angle: (a) frequency distribution, and (b) trends in the mean anomalies for NOAA-16 and -17.

Note that the MUT processing is based on 2×2 GAC pixel arrays, resulting in an effective resolution of a SSTOBS/AEROBS “pixel” of ~ 8 km. However, the SST/AOD data are void in many areas due to cloud. Therefore, 50/100km analyzed SST/AOD fields are also generated as a part of the MUT system and published daily at <http://www.osdpd.noaa.gov/PSB/EPS/EPS.html>.

5. NOAA16/17 SST AND AEROSOL PRODUCTS

For the analyses below, the 8-km AEROBS data from 3-11 December 2003 have been first averaged into $1 \text{ day} \times (1^\circ)^2$ space-time boxes, resulting in $N=62,197$ and $56,054$ grids for NOAA-16 and -17, respectively. The observed $\sim 11\%$ difference in a sample size between the AM and PM platforms may be due to a diurnal cycle in cloud cover. Or, it may result from the fact that calibration of the AVHRR SRBs used for cloud screening may be offset between the two platforms (see discussion of the aerosol product in section 5.2 below).

The NOAA-16 and -17 samples overlap in a sub-sample called *intersection* (in which both NOAA-16 and -17 data retrievals are available). There are $N=17,728$ $1 \text{ day} \times (1^\circ)^2$ such grids ($\sim 30\%$ of the full samples). In $N=44,469$ grids, NOAA-16 data are available but NOAA-17 are not; this sub-sample is called the NOAA-16 *complement*. In $N=38,326$ grids, NOAA-17 data are available but NOAA-16 are not; this sub-sample is called the NOAA-17 *complement*.

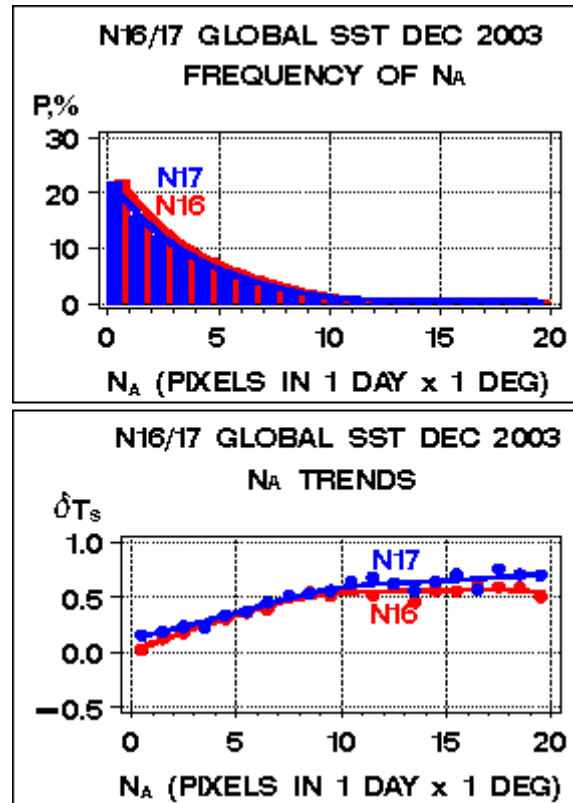


Fig.9. Count of clear-sky pixels within $1 \text{ day} \times (1^\circ)^2$: (a) frequency distribution, and (b) trends in the mean δT_s .

Each AEROBS data record includes lat/lon, day, LT, sun and view zenith, and relative azimuth angles, reflectances in the SRBs and brightness temperatures in the EEBs, NLSST (T_s), and 3 AODs (τ). On NOAA-16, band 3A was discontinued in May 2003 and thus τ_3 is not available.

The operational NLSST coefficients are found at <http://manati.web.noaa.gov/sst/cwlIntroduction.html>. These have been derived empirically using least square linear regression against buoy measurements as documented in Li et al. (2001). A monthly mean $(1^\circ)^2$ ground-based conventional climatological SST, T_c , (Robinson and Bauer 1985) is available only in a subset of the AEROBS points ($N=60,140$ and $53,963$ for NOAA-16 and -17, respectively). In those points, SST anomalies have been calculated as $\delta T_s = T_s - T_c$. The *intersection*, and NOAA-16 and -17 *complements* sub-samples of the anomalies contain $N=17,032$, $43,108$, and $36,931$ $1 \text{ day} \times (1^\circ)^2$ grids, respectively.

5.1 SST Retrievals

Figure 4 shows global maps of T_s derived from NOAA-16 and -17, and Figure 5 plots results of their statistical analyses.

Global frequency distributions of T_s in Fig.5a are highly skewed. The two statistics are well reproducible from the two platforms. Counter-intuitively, the morning NOAA-17 reveals a warm bias of $\sim +0.3\text{K}$ relative to the

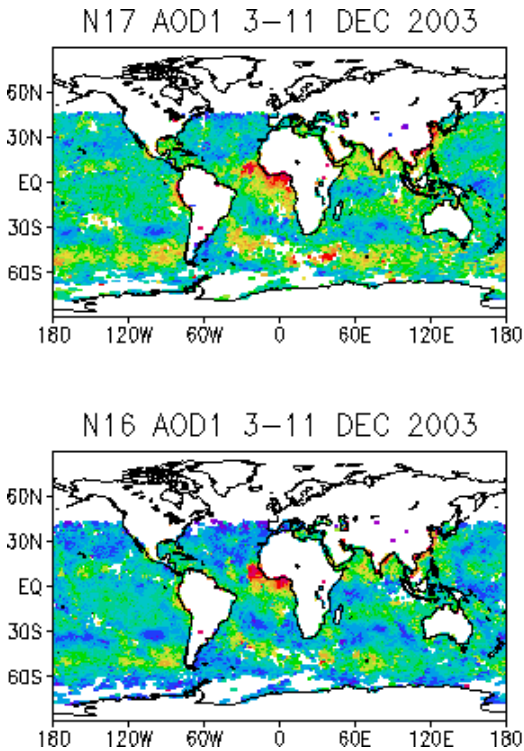


Fig.10. Global distribution of aerosol optical depth in AVHRR/3 band 1, τ_1 ($\lambda_1=0.63 \mu\text{m}$), in December 2003.

afternoon NOAA-16. This bias is deemed to be due to different sampling as it largely disappears in Fig.5b, which plots frequency distributions of the cross-platform T_S difference, $\Delta T_S \equiv T_{16} - T_{17}$. This difference can be calculated only in the *intersection* sub-sample, which is common to the two platforms. The frequency distribution of ΔT_S is nearly-symmetric and close to Gaussian, with $\sigma \sim 0.70\text{K}$. The latter number can be used to estimate the RMS error (noise) in the $1\text{day} \times (1^\circ)^2$ NLSST product. Assuming that contributions to this error are comparable from the two platforms and independent, one obtains that $\sigma_N \sim \sqrt{\sigma^2/2} \sim 0.49\text{K}$. The correlation between the T_{16} and T_{17} in the *intersection* sub-sample is shown in Fig.5c. The R^2 is ~ 0.993 , and the RMSD is $\sigma \sim 0.69\text{K}$. [Note that $\sigma \sim 0.69\text{K}$ is reduced from $\sigma \sim 0.70\text{K}$ for the temperatures, due to a reduced anomalies sample size, as a result of points for which the Robinson-Bauer (1985) T_C data are not available.]

If any *a priori* information on the SST distribution on our planet Earth was lacking, then Fig.5 would have served to specify the *a priori* uncertainty in the SST to be narrowed down by remote sensing measurements. Taking, for the sake of estimate, the RMSD in Fig.5a, $\sigma \sim 8.5\text{K}$ as a definition of such SST signal, and comparing it to the SST noise estimated above $\sigma_N \sim 0.5\text{K}$ one can estimate a *signal-to-noise ratio* (SNR) as $\xi \sim (8.5\text{K}/0.5\text{K}) \sim 17$, an excellent information content of the remote sensing technique.

However, prior climatological knowledge on the SST is available, and the objective of the SST remote sensing may be viewed as estimating the deviation from

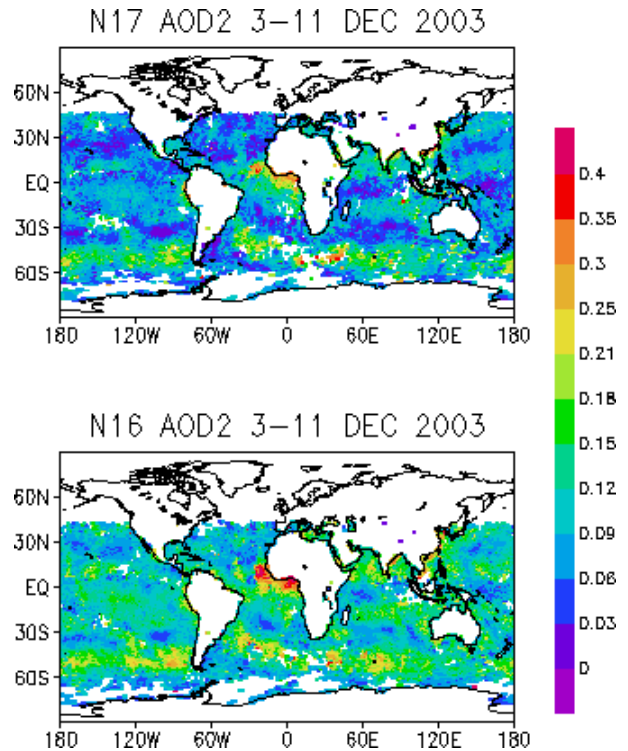


Fig.11. Same as in Fig.10 but for AOD in AVHRR/3 channel 2, τ_2 ($\lambda_2=0.83 \mu\text{m}$).

the expected state. To that end, Fig.6 re-plots global T_S maps from Fig.4 as δT_S -maps. The two patterns of anomalies look very similar, and the δT_S -histograms in Fig.7a match each other even more closely than the T_S -histograms in Fig.5a (in particular, the cross-platform difference is reduced to $< 0.1\text{K}$). Although histograms of the anomalies are expected to be centered at zero, both have a slightly-positive offset of $\sim (0.30 \pm 0.04)\text{K}$. The cause of this warm bias in the NLSST relative to the Robinson-Bauer (1985) climatology will be explored in the future. The RMSD is $\sigma_o \sim 1\text{K}$, with NOAA-16 showing somewhat larger SST variability. The R^2 is ~ 0.59 , which is a significantly lower correlation than in the SSTs. This is expected as the largest variability, determined by the SST geographical distribution, has been removed from the data. Note that the smaller bias and RMSD in Figs. 7ab compared to Figs. 5ab for the SSTs is likely due to the removal of some marginal data points with missing climatological SST from the data.

Remarkably, the δT_S -frequency distributions in Fig.7b are of near-gaussian shape, and not only geophysically but also statistically seem to be more adequate to define the SST *signal* than those in Fig.5b. Note that the RMSD in Fig.7a of $\sigma_o \sim 1\text{K}$, in addition to the physical anomaly *signal*, also has a contribution from at least two other components: noise in the satellite retrievals, σ_N , and RMS errors in the (Robinson-Bauer 1985) climatology, σ_C . [Note that in addition to possible uncertainties in the Robinson-Bauer T_C , the MUT system may also contribute some noise, as it does not interpolate the monthly $1^\circ T_C$ climatology in space and

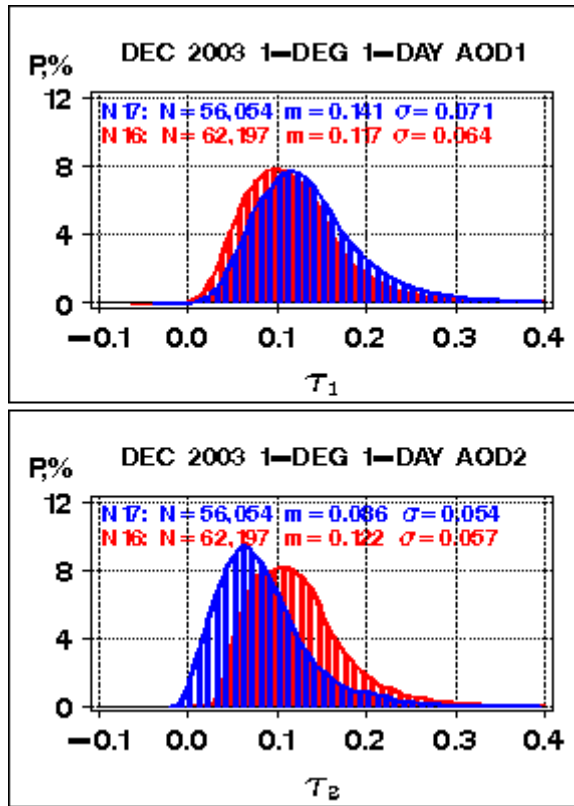


Fig.12. Global histograms of AODs in AVHRR channels 1 and 2, $\tau_1(\lambda_1=0.63 \mu\text{m})$ and $\tau_2(\lambda_2=0.83 \mu\text{m})$.

time, but rather uses a closest grid value.] If all three components are independent and add up in a RMS sense, then: $\sigma_o = \sigma_s^2 + \sigma_N^2 + \sigma_C^2$. Neglecting contribution from σ_C^2 , and estimating σ_N from the $\sigma=0.69\text{K}$ in Fig.7b as $\sigma_N \sim \sqrt{(0.69\text{K})^2/2} \sim 0.49\text{K}$, one arrives at the estimate of the signal: $\sigma_s \sim 0.87\text{K}$. Combining the signal and noise estimates together, the SNR is estimated as $\xi \sim \sigma_s/\sigma_N \sim (0.87/0.49) \sim 1.78$, which is almost an order of magnitude smaller compared to the $\xi \sim 17$ obtained from the SSTs.

Note that the σ_s , σ_N , and ξ numbers listed above are representative of globally-average conditions. In reality, the anomaly signal, σ_s (such as the climatological σ_{TS} , characterizing, e.g., SST inter-annual variability) varies in space and time, and the algorithmic RMS accuracy, σ_N , depends upon retrieval conditions (e.g. atmospheric water vapor, aerosol, and temperature profiles, residual cloud, and view geometry in the retrieval point). Therefore it is expected that the efficacy of the retrieved SST is also a function of location, season, and retrieval conditions. For instance, in the tropics, the SST natural variability is smallest whereas the errors of the remote sensing techniques is expected to be largest due to a strongest atmospheric hindrance, and therefore the SNR is expected to be smallest.

The current NESDIS SST product is deemed to have some room for improvement. For example, if the global average σ_N is lowered to 0.30K , then the global-average SNR would be $\xi \sim (0.87\text{K}/0.30\text{K}) \sim 3$. Note

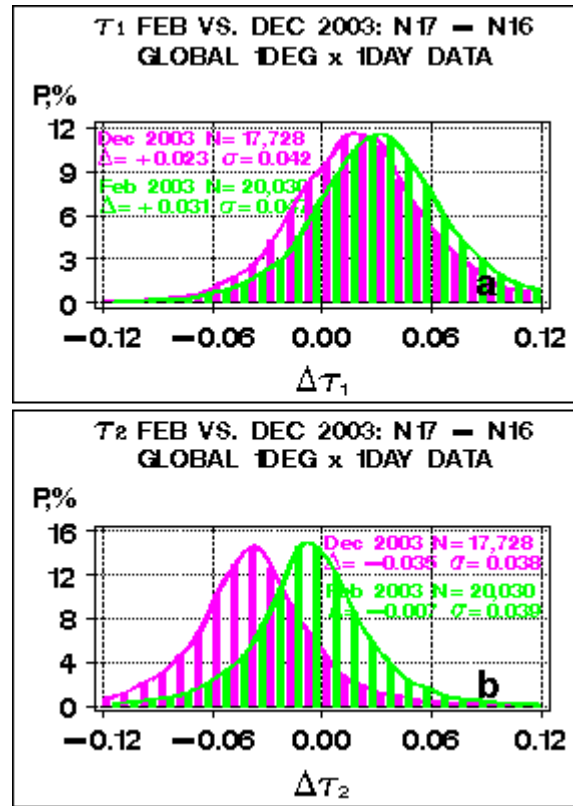


Fig.13. "NOAA-17 minus NOAA-16" τ -differences in December (magenta) and February (green) 2003.

however that the improvement if achieved may be not regionally and/or seasonally uniform.

There are a number of potential areas where the SST accuracy can be improved. Figs.8-9 illustrate two of them. It has been observed that the SST algorithms perform non-uniformly over the full range of view angles (Llewelyn-Jones 1984; McClain et al. 1985). Figure 8 quantifies this effect in the NESDIS NLSST which corrects for the view angle effect, empirically (Walton et al. 1998). Beyond $\sim 40^\circ$ view angle, a negative bias develops and reaches $\sim -0.5\text{K}$ at the edge of the scan (recall that the current NLSST retrievals are not made beyond 60°). The cause of the elevated δT_s near nadir in the NOAA-17 data (collocated with the dip in the view angle frequency distribution) is not immediately clear. Figure 9 plots the mean SST anomaly as a function of count of clear-sky pixels in a $1\text{day} \times (1^\circ)^2$ box, N_A . The latter is used as a proxy of the (inverse) cloud amount (which is missing from the current MUT processing). The smaller N_A , the higher the ambient cloud, and the larger the negative bias in T_s , reaching -0.5K at $N_A=1$. Note that the vast majority of data points are found in the $N_A < 10$ domain where the bias is noticeable and variable. This cloud bias in the retrieved SST may be real (i.e., result from the surface cooling in the presence of larger ambient cloud). Or, it may result from the residual cloud in a field of view. Analyses of buoy data are underway to attribute these two causes.

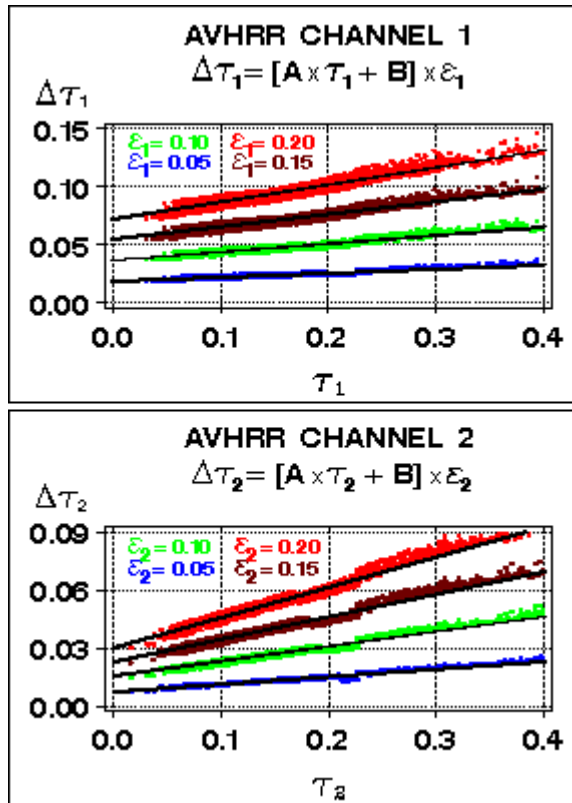


Fig.14. Error in AOD, $\Delta\tau$, caused by error in calibration slope, ϵ (after Ignatov 2002.)

5.2 Aerosol Retrievals

In February 2003, Ignatov et al. (2004a) had performed analyses similar to the December 2003 analyses presented here. In what follows, the two results obtained with a 10-month time lag are contrasted against each other as appropriate.

Figures 10-11 map the distribution of AOD over the global ocean, derived from two AVHRR channels on the two platforms and Fig.12 plots their global histograms. [Note that NOAA-17 τ_3 is available but not analyzed here as its NOAA-16 counterpart is not available.]

The shape of the τ -histograms is close to log-normal as expected (O'Neill et al. 2000; Ignatov and Stowe 2002b; Ignatov and Nalli 2002). Mean τ 's are superimposed in Fig.12 $\tau_{1,16} \sim 11.7 \times 10^{-2}$, $\tau_{1,17} \sim 14.1 \times 10^{-2}$, $\tau_{2,16} \sim 12.2 \times 10^{-2}$, $\tau_{2,17} \sim 8.6 \times 10^{-2}$ (cf. with $\tau_{1,16} \sim 12.0 \times 10^{-2}$, $\tau_{1,17} \sim 15.0 \times 10^{-2}$, $\tau_{2,16} \sim 10.2 \times 10^{-2}$, and $\tau_{2,17} \sim 10.3 \times 10^{-2}$ for February 2003). Cross-platform differences in December 2003 are shown in Fig.13, and contrasted against February 2003. All histograms would center at zero if there were no systematic errors in τ . Based on an observation that there is no regularity in the τ -changes between bands and platforms, Ignatov et al. (2004a) concluded that the AVHRR/3 calibration uncertainty is the most plausible cause, not aerosol physics or retrieval algorithm. Note that the diurnal effect in AOD over ocean is small (Kaufman et al. 2000). Temporal changes are also detected, but they are generally

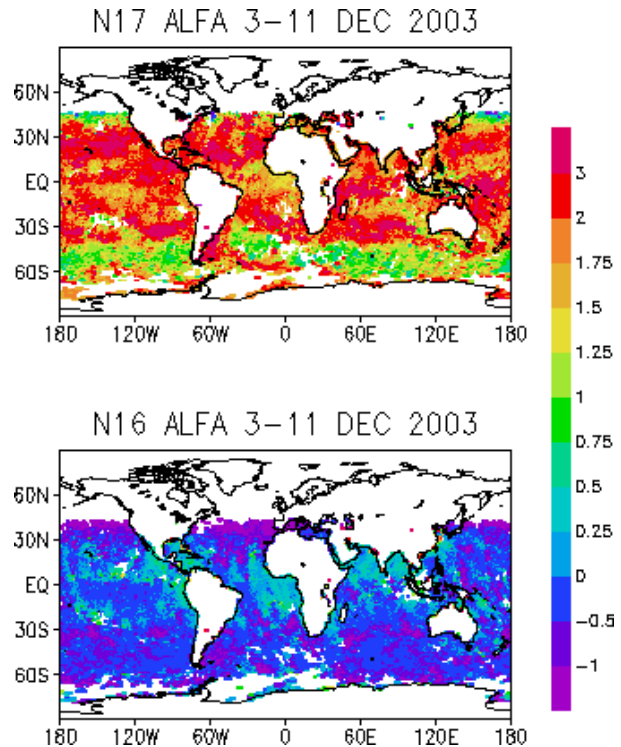


Fig.15. Global distribution of the Angstrom exponent derived as $\alpha = -\ln(\tau_1/\tau_2)/\ln(\lambda_1/\lambda_2)$.

smaller than cross-platform differences, and subject to larger sampling differences. For instance, the December and February 2003 *intersection* sub-samples from which Fig.13 was derived, may sample different parts of the global ocean, and some inter-annual change in aerosol loading may also occur. Greater care must be exercised in the global τ -time series analyses.

To facilitate the interpretation of the observed cross-platform τ -differences in terms of the equivalent calibration slope changes, Fig.14 plots sensitivity charts of AOD errors, $\Delta\tau$, to calibration slope errors, ϵ , after Ignatov (2002). For typical values of $\tau_1 \sim \tau_2 \sim 0.1$ over ocean, observed τ -differences in December 2003 are equivalent to cross-platform gain offsets (NOAA-17 minus NOAA-16) of $\epsilon_1 \sim +5\%$ in band 1, and $\epsilon_2 \sim -8\%$ in band 2 (cf. with $\epsilon_1 \sim +4\%$ and $\epsilon_2 \sim -2\%$ in February 2003). These estimates are preliminary and require further checking. The uncertain and unstable calibration gain is the major challenge in the operational aerosol retrievals from AVHRR. In a different perspective, the aerosol product has a clear potential to contribute to narrowing down the uncertainty in the calibration gain. Note that errors in AOD may be caused not only by the erroneous calibration slope, but also by an incorrect intercept (Ignatov et al. 2004a,e). Ignatov et al. (2004e) argue that the AVHRR space count measurements should be used to constrain its calibration offset.

Figure 13 also allows an estimate of the noise in the $1\text{day} \times (1^\circ)^2$ τ -product. As with the SST analyses, we assume that the random τ -errors from the two platforms are independent and comparable, to obtain an estimate

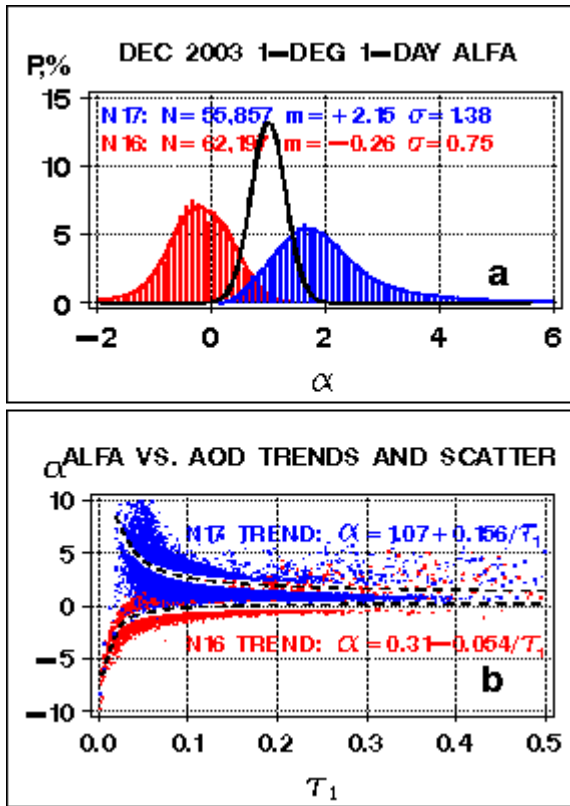


Fig.16. Histograms of the Angstrom exponent, α , and scattergrams of α vs τ .

of noise as $\sigma_{N_{\tau 1}} \sim \sqrt{(4.5 \times 10^{-3})^2 / 2} \sim 3.2 \times 10^{-3}$ in band 1, and $\sigma_{N_{\tau 2}} \sim \sqrt{(3.8 \times 10^{-3})^2 / 2} \sim 2.7 \times 10^{-3}$ in band 2. This noise is to be compared to the τ -signal in Fig.12. Defining the signal-to-noise ratio is however not straightforward here as the τ -signal is log-normal and the τ -noise is normal. Calculating τ -anomalies is impossible as τ -climatology is not yet available.

Global distribution of the Angstrom exponent, $\alpha = \ln(\tau_1/\tau_2) / \ln(\lambda_1/\lambda_2)$, from the two platforms is shown in Fig.15, and their respective frequency distributions are plotted in Fig.16a. Typically, α is expected to be distributed normally, to fall in a range from 0-2, and peak at $\alpha \sim 0$ to 1. This hypothetical distribution is superimposed in Fig.16a as a black solid line. However, the actual α deviates from a Gaussian shape, and it is biased low by $\Delta\alpha > 1$ in the NOAA-16 data and high by $\Delta\alpha > 1$ in the NOAA-17 data. For NOAA-16, there is a significant deterioration in α between February 2003 and December 2003, with the mean α decreasing from a reasonable value of $\sim +0.5$ to -0.3 . For NOAA-17, α remained almost unchanged and unreasonable ($+2.29$ in February, and 2.15 in December 2003), indicating either little or a coherent change in the AVHRR solar reflectance bands.

Fig.16b shows " α vs. τ " trends in the NOAA-16 and -17 data. They are significant and opposite, indicating significant data errors in the τ -data derived from both

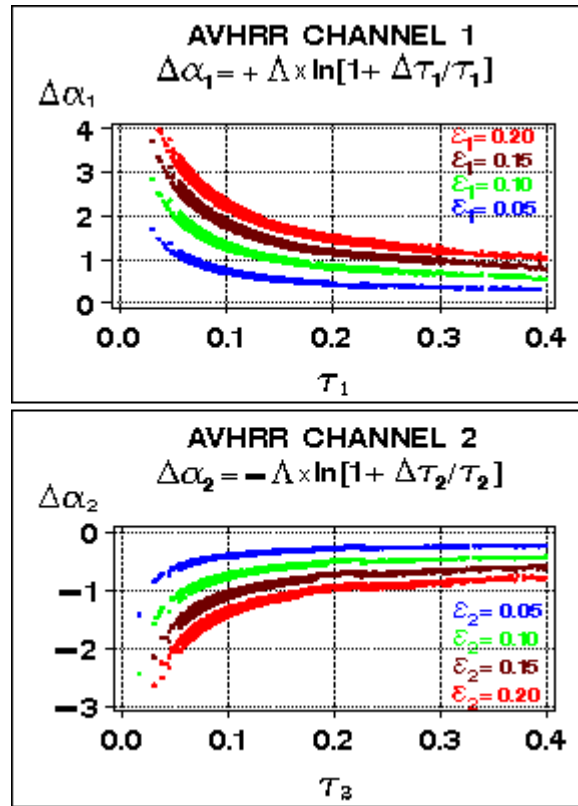


Fig.17. Calibration slope-induced error in the Angstrom exponent (after Ignatov 2002).

platforms (Ignatov and Stowe 2002b; Ignatov and Nalli 2002; Ignatov et al. 2004a).

Fig.17 plots the α -sensitivity charts after Ignatov (2002) similar to the τ -charts in Fig.14. For typical $\tau \sim 0.1$ over ocean, a 5-10% calibration difference can easily cause the observed differences in the Angstrom exponent, which is known to be very sensitive to τ -errors, especially at low AODs (Ignatov et al. 1998).

5.3 Aerosol/SST Correlations

Aerosols are known to affect the SST retrievals in the thermal IR (Strong et al. 1983). Griggs (1985) derived simple theoretical equations to predict the aerosol effect on AVHRR channel 4 and 5 brightness temperatures, T_4 and T_5 :

$$\Delta T_4 = A_4 \tau_{a4} \sec \theta, \quad \Delta T_5 = A_5 \tau_{a5} \sec \theta \quad (1)$$

In Eq.(1), θ is the view zenith angle, and τ_{ai} are absorbing AODs in AVHRR channels $i=4$ and 5. These thermal IR AODs should not be confused with the AODs τ_1 and τ_2 , analyzed in section 5.2, which are scattering AODs, and derived in AVHRR bands 1 and 2, separated from bands 4 and 5 in spectrum by $\sim 10 \mu\text{m}$. The proportionality coefficients, A_i , generally depend upon spectral interval, but they are mostly functions of T_S (surface temperature) and T_A (aerosol temperature):

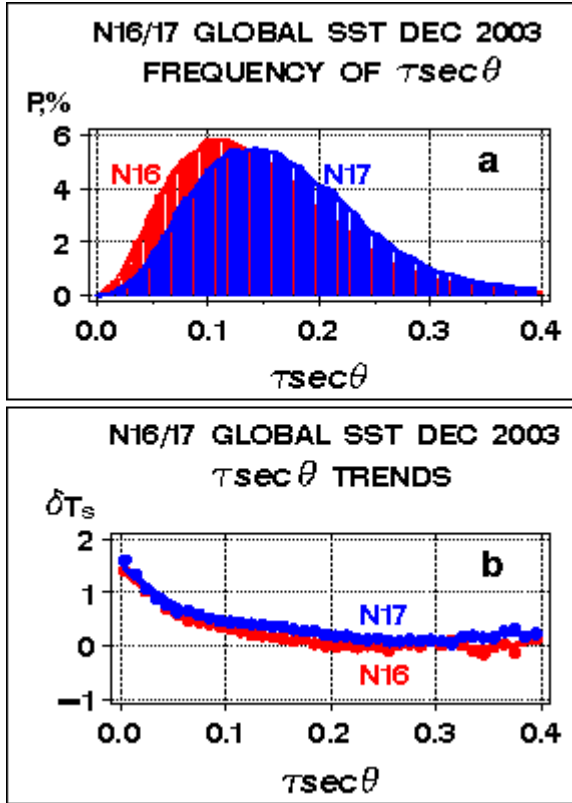


Fig.18. (a) Histograms of slant-path AOD in AVHRR channel 1, $\tau_1 \text{sec}\theta$, and (b) trends in SST anomalies.

$$A_i = \left[B(T_s) - B(T_A) \right] \frac{\partial T}{\partial B(T_s)} \approx T_s - T_A \quad (2)$$

The latter approximate equality in Eq.(2) holds when the aerosol layer is in the troposphere and close to the surface, so that its temperature, T_A , does not differ significantly from the surface temperature, T_s . This is probably representative of the typical conditions in December 2003 when no high-level stratospheric aerosol layer was observed.

The aerosol-induced bias in the derived SST is estimated by substituting ΔT_4 and ΔT_5 from Eq.(1) into an SST retrieval equation such as the MCSST or NLSST. If the aerosol spectral dependence were similar to that of water vapor, then the aerosol effect in the two brightness temperatures would cancel out. However, the spectral dependencies of water vapor and aerosol in the window region are generally opposite: absorption water vapor increases with wavelength whereas the aerosol signals decreases (e.g. Griggs 1985; Walton 1985; Merchant et al. 1999). As a result, the disturbing effect of aerosol is amplified by the MC/NLSST. There are two major ways to deal with aerosol contamination in the SST. One is to utilize the unique information potential of the three AVHRR EEBs and tune the three-channel algorithm to remove effects of both water vapor and aerosol. This approach was explored e.g. by Walton (1985) and Merchant et al. (1999). It cannot be utilized during daytime however when AVHRR band 3 is

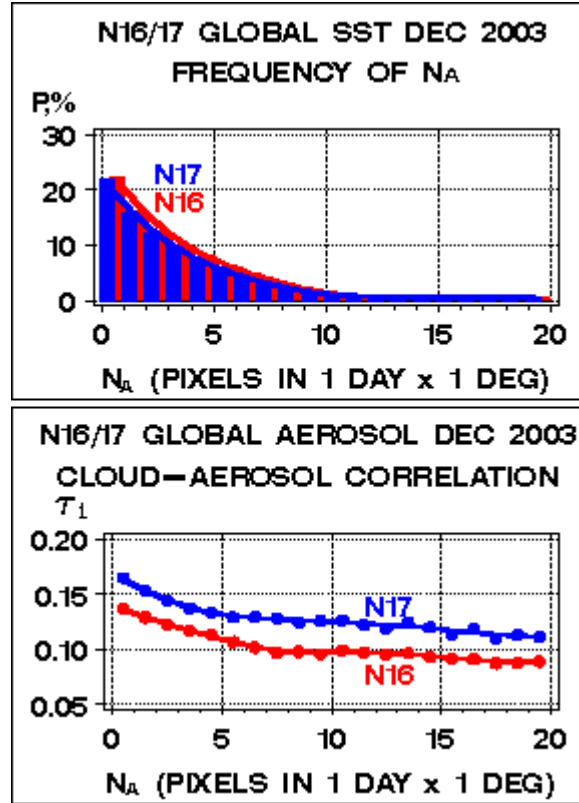


Fig.19. (1) Count of aerosol pixels within $[1\text{day} \times (1^\circ)^2]$ boxes, N_A (centered at $\Delta N_A=1$), and trends in τ_1 .

contaminated by reflected solar light. The other approach is to utilize the visible AODs (τ_1 or τ_2) to predict the τ_4 and τ_5 assuming the aerosol spectral dependence (model) non-variable. This approach was explored for instance by Griggs (1985), May et al. (1992), and Nalli and Stowe (2002). Eq.(1) suggest that the SST correction term should be linear with respect to the slant-path AOD in band 1 or 2, $\tau_1 \text{sec}\theta$ or $\tau_2 \text{sec}\theta$.

Note however that in addition to the assumption of a non-variable aerosol model, another assumption is also made (often, implicitly). According to Eqs.(1-2), ΔT_i are proportional to an unresolved combination of two factors: (1) aerosol amount, τ , and (2) its vertical placement as defined by the temperature difference, $T_s - T_A$. When AOD is used as the only predictor in the correction, it is assumed that global aerosol is located at approximately the same altitude in the atmosphere, so that its temperature contrast with the surface is non-variable, i.e. $T_s - T_A \approx \text{const}$, leading to the need to separate the aerosol into stratospheric (volcanic) and tropospheric (background) modes (e.g. Griggs 1985; May et al. 1992; Walton 1985; Nalli and Stowe 2002).

As a preliminary test with the AEROS data, Fig.18 shows a correlation of the SST anomaly versus slant-path AOD in AVHRR channel 1. Trends from the two platforms are in a remarkable agreement, but they deviate from the expected pattern when the correction looks as a straight line intersecting the origin. Griggs (1985) and Nalli and Stowe (2002) argued that since the

operational SST equations are empirically tuned to the average atmospheric conditions (i.e. those that include background tropospheric aerosol) the aerosol-induced bias should be near average anomaly $\delta T_S + 0.3K$ (cf. Fig.7a) at the typical aerosol conditions (represented by a modal value of $\tau_1 \sec \theta \sim 0.13-0.15$) and not at $\tau_1 \sec \theta \sim 0$. [Note that the two histograms of $\tau_1 \sec \theta$ are shifted with respect to each other, due to the calibration differences discussed in section 5.2.] Indeed, aerosol correction to the SST greatly diminishes in the vicinity of the $\tau_1 \sec \theta$ -mode. It is somewhat counter-intuitive that the dependence of δT_S vs. $\tau_1 \sec \theta$ is non-linear: it picks up at smaller $\tau_1 \sec \theta$, and flattens out at higher values of $\tau_1 \sec \theta$. Note that the linearity of the δT_S vs. $\tau_1 \sec \theta$ relationship assumes that AODs are located at approximately the same altitude, which may not be the case. The observed non-linearity may thus be related to the fact that different AODs reside on different levels in the atmosphere. Note that Griggs (1985) also observed a non-linearity, but did not offer any explanation.

Another possible explanation of the observed non-linearity may be due to the fact that the satellite-derived AOD may be subject to residual cloud. Fig.19 shows that AOD reveals cloud trends similar to those documented in Fig.9 for the SST. These trends have been previously observed in aerosol retrievals from a number of sensors and platforms (Ignatov and Nalli 2002; Ignatov et al. 2004 b,c). Griggs (1985) points out that a ($\tau \sec \theta$) correction also removes some residual cloud in a satellite field-of-view. (Note that although the correction to the BTs from a residual cloud may be well described by Eqs.(1-2), the cloud may be found at a different elevation above the surface and therefore have a different temperature, T_A)

More research is needed to better understand the effect of aerosol on IR channel brightness temperatures for deriving improved radiative-transfer-based or empirical SST correction algorithms.

6. CONCLUSION

The SST and aerosol products from AVHRR at NESDIS are derived from the same sensor, and within the same processing system called MUT. This processor is currently under a fundamental redesign. It is appropriate at this time to review the two products and analyze them synergistically. These analyses are also helpful to highlight the specific features of each product, and to emphasize their inter-relationships and inter-dependencies.

The SST is derived from the AVHRR Earth emission bands which are well-calibrated onboard. As a result, the SST parameter from the AVHRR is relatively accurate, and well-reproducible from the two operational platforms. In a global sense, the errors in the SST product are mainly random (although they may be localized regionally and/or seasonally). According to our estimate here, this noise is $\sigma_N \sim 0.50K$.

The SST is subject to the diurnal cycle, and therefore time differences between the two platforms may contribute to the cross-platform "noise". The skin SST retrieved from space is also known to differ from

the bulk SST measured by buoys. Merging the satellite data with the National Centers for Environmental Prediction (NCEP) forecast fields is underway to model the skin-bulk difference in the ocean boundary layer and throughout the diurnal cycle. The NCEP upper air data will also help to constrain the parameters in the atmospheric correction algorithms.

The aerosol product, on the other hand, is derived from the solar reflectance bands which are not calibrated onboard. As a result, the AVHRR aerosol product is subject to significant systematic errors (up to $\Delta \tau \sim (3-5) \times 10^{-2}$ in band 1), which may additionally change in time as the calibration slopes in the AVHRR SRBs degrade. Note that the cross-platform noise was found to be $\sigma_{N\tau 1} \sim 3.2 \times 10^{-3}$ and $\sigma_{N\tau 2} \sim 2.7 \times 10^{-3}$ in bands 1 and 2, respectively. These errors should be compared against the typical AOD signal over ocean $\tau_1 \sim \tau_2 \sim 0.10-0.15$.

The foremost issue with the NESDIS aerosol product is the AVHRR calibration. Until an accurate and stable solution is found for the AVHRR calibration, the continued use of a single-channel methodology is recommended to remain in place for the four Initial Joint POES System (IJPS) platforms (NOAA-N, and METOP-1 to 3) that carry the AVHRR/3 instrument. One should keep in mind the qualitative, real-time nature of the NESDIS aerosol product, and care is advised in their quantitative analyses and use (e.g., for the aerosol correction for SST).

Another specific feature of the two products is that the expected state is well-established for SST (climatology) but not for the AOD. The availability of an expected SST state largely facilitates the evaluation of the derived SST product. On the other hand, the lack of aerosol climatology complicates any evaluation of the aerosol product. Development of an aerosol climatology is thus a high priority task. The task of creating climatology for aerosol is more complex than for the SST for a number of reasons. Data over the open ocean are much more scarce and of a short-term nature for the aerosols. Aerosol is a multi-factor parameter, whose compressed representation is yet to be developed. Aerosol optical depth is distributed log-normally, and ways should be sought to design its climatology. On the other hand, the SST is a scalar parameter which is distributed normally. Note that in reality, SST is a function of the diurnal time and depth, and effort should be aimed at developing a diurnal-cycle and ocean-depth resolved climatology, in terms of a mean expected state and variability about the mean. This task is currently pursued under the GODAE Project (<http://www.ghrsst-pp.org>.)

We emphasize the importance of development and application of comprehensive self- and cross-consistency checks to the global SST and aerosol products, examples of which have been illustrated in this study. These provide a valuable supplement to the traditional validation against buoy SST and sun-photometer aerosol measurements which are not available globally.

These analyses are currently underway at NESDIS, and their results will be reported in future work.

Acknowledgment. The SST, aerosol, and cloud products from AVHRR were initiated at NESDIS in the 1980s by P. McClain, L. Stowe, C. Walton (all retired) and N. Rao (deceased). The aerosol product has been enhanced and applied to other sensor data (TRMM VIRS, Terra/Aqua MODIS, and MSG SEVIRI) under the CERES project. We are indebted to C. Cao, A. Heidinger, J. Sullivan, and F. Wu (NESDIS) for helpful discussions. This work was funded under the NASA/CERES, NOAA Polar System Development and Implementation (PSDI), NOAA/NASA/DOD Integrated Program Office, NOAA Ocean Remote Sensing, and the Joint Center for Satellite Data Assimilation Programs. We thank M. Mignogno and T. Schott (NOAA), S. Mango (IPO), J. LeMarshall and F. Weng (NESDIS) for their support and encouragement. The views, opinions, and findings contained in this report are those of the authors and should not be construed as an official NOAA or U.S. Government position, policy, or decision.

References

- Goodrum, et al., 2003: NOAA-KLM Users Guide, NOAA/NESDIS, 1106 pp [Available from NCDC, 151 Patton Ave., Asheville, NC 28801-5001; online <http://www2.ncdc.noaa.gov/docs/klm/index.htm>].
- Griggs M., 1975: Measurements of atmospheric aerosol optical depth over water using ERTS-1 data. *J. Air Poll. Control Assoc.*, **25**, 622-626.
- Griggs M., 1985: A method to correct satellite SST for the effects of atmospheric aerosols, *JGR*, **90**, 12,951-12,959.
- Ignatov A., et al, 2004a: Operational Aerosol Observations (AEROBS) from AVHRR/3 onboard NOAA-KLM satellites. *JTech.*, **21**, 3-26.
- Ignatov A., et al, 2004b: Two MODIS aerosol products over ocean on the Terra and Aqua CERES SSF datasets. *JAS*, in press.
- Ignatov A., et al, 2004c: Aerosol retrievals from TRMM/VIRS over open oceans. *JAM*, in prep.
- Ignatov A., et al, 2004d: Equator crossing times for NOAA, ERS, and EOS sun-synchronous satellites. *Int. J. Remote Sensing*, in press.
- Ignatov A., et al, 2004e: The usefulness of in-flight measurements of space count to improve calibration of the AVHRR solar reflectance bands. *JTech.*, in press.
- Ignatov A., 2002: Sensitivity and information content of aerosol retrievals from AVHRR: Radiometric factors. *Appl. Opt.*, **46**, 6, 991-1011.
- Ignatov A., and N. Nalli, 2002: Aerosol retrievals from multiyear/satellite AVHRR PATMOS dataset for correcting remotely sensed SST. *JTech.*, **19**, 1986-2008.
- Ignatov A., and L. Stowe, 2002a: Aerosol retrievals from individual AVHRR channels: I. Retrieval algorithm and transition from Dave to 6S radiative transfer model. *JAS*, **59**, 3(1), 313-334.
- Ignatov A., and L. Stowe, 2002b: Aerosol retrievals from individual AVHRR channels: II. Quality control, PDFs, information content, and consistency checks of retrievals. *JAS*, **59**, 3(1), 335-362.
- Ignatov A. et al., 1998: Sensitivity study of the Ångström exponent derived from AVHRR over oceans. *Adv. Space Res.*, **21**, 3, 439-442.
- Kaufman Y., et al, 2000: Will aerosol measurements from Terra and Aqua polar orbiting satellites represent the daily aerosol abundance and properties? *GRL*, **27**, 3861-3864.
- Kidwell, K. (Ed.), 1998: NOAA polar orbiter data user's guide, NOAA/NESDIS, 394 pp. (Available from NCDC, 151 Patton Ave, Asheville, NC 28801-5001, <http://www2.ncdc.noaa.gov/docs/podug/index.htm>).
- Li, X., et al., 2001: Deriving the operational nonlinear multichannel sea surface temperature algorithm coefficients for NOAA-15 AVHRR/3, *Int. J. Remote Sensing*, **22**, 4, 699-704.
- Llewellyn-Jones D., et al., 1984: Satellite multi-channel IR measurements of SST of the N.E. Atlantic Ocean using AVHRR/2. *QJRMMS*, **110**, 613-631.
- May D., et al., 1992: A correction for Saharan dust effects on satellite SST measurements. *JGR*, **97**, 3611-3619.
- May D., et al., 1997: Operational processing of satellite SST at NAVOCEANO. *BAMS*, **79**, 397-407.
- McClain P., 1989: Global sea surface temperatures and cloud clearing for aerosol optical depth estimates, *Int. J. Remote Sensing*, **10**, 763-769.
- McClain P., et al, 1985: Comparative performance of AVHRR based multichannel sea surface temperatures, *JGR*, **90**, 11587-11601.
- McMillin L., 1975: Estimation of SST from two IR window measurements with different absorption. *JGR*, **80**, 5113-5117.
- Merchant C., et al., 1999: Toward the elimination of bias in satellite SST: I. Theory, modeling, inter-algorithm comparison, *JGR*, **104**, 23,565-23,578.
- Nalli, N., and L. Stowe, 2002: Aerosol correction for remotely sensed SSTs from the NOAA AVHRR. *JGR*, **107**, 3172, doi:10.1029/2001JC00162.
- O'Neill et al., 2000: The log-normal distribution as a reference for reporting AOD statistics; Empirical tests using multi-year, multi-site AERONET sun photometer data. *GRL*, **27**, 3333-3336.
- Rao N. and J. Chen, 1995: Inter-satellite calibration linkages for the visible and near-infrared channels of AVHRR on the NOAA-7, -9, and -11 spacecraft. *Int. J. Remote Sens.*, **16**, 1931-1942.
- Rao N., et al., 1989: Remote sensing of aerosols over oceans using AVHRR data. *Int. J. Remote Sens.*, **10**, 743-749.
- Robinson M. and A. Bauer, 1985: Description of the Bauer-Robinson numerical atals, ver. VIII, Feb 1985, <http://dss.ucar.edu/datasets/ds278.0>
- Strong, A., et al., 1983: Using the NOAA7 AVHRR to monitor El Chichon aerosol evolution and subsequent SST anomalies, Proc. 17th Int. Symp. Remote Sensing Env., An Arbor, MI.
- Walton C., 1985: Satellite measurement of SST in the presence of volcanic aerosols, *JCAM*, **24**, 501-507.
- Walton C., et al., 1998: The development and operational application of non-linear algorithms for the measurement of SST from the NOAA POES. *JGR*, **103**, 27999-28012.